

Novel Long Short-Term Memory Cell Architectures: Application to Light Field Face Recognition

Alireza Sepas-Moghaddam^a, Fernando Pereira^a and Paulo Lobato Correia^a

^a Instituto de Telecomunicações, Instituto Superior Técnico – Universidade de Lisboa, Torre Norte, Av. Rovisco Pais, Lisbon 1049-001, Portugal
{alireza, plc, fp}@lx.it.pt}

Abstract

Long Short-Term Memory (LSTM) is a prominent recurrent neural network for extracting dependencies from sequential data, having achieved impressive results for different visual recognition tasks. With the emergence of lenslet light field cameras able to capture rich spatio-angular information from multiple directions, new frontiers in visual recognition performance have been opened. Since multiple 2D viewpoint images can be rendered from a light field, those multiple images, or descriptions extracted from them, can be organized as a pseudo-video sequence so that a LSTM network learns a model describing that sequence. However, this architectural approach using the conventional LSTM cells does not fully exploit, during the learning process, the inter-view angular information captured by the light field image. This paper proposes three novel LSTM cell architectures able to create richer and more effective description models for visual recognition tasks, by jointly learning from two sequences simultaneously acquired. The novel key idea is to jointly process two sequences of rendered 2D images or their descriptions, e.g. representing the scene horizontal and vertical parallaxes, and thus with some specific dependency between them, that would not be exploited otherwise. To show the efficiency of the novel LSTM cell architectures, these architectures have been integrated into an end-to-end deep learning face recognition framework, which creates this joint spatio-angular light field description. The LSTM network, using the proposed LSTM cell architectures, receives as input a sequence of VGG-Face descriptions computed for parallax related, horizontal and vertical 2D face viewpoint images, derived from the input light field image. A comprehensive evaluation in terms of recognition accuracy, computational complexity, memory efficiency, and parallelization ability has been performed with the IST-EURECOM LFFD database using three new and challenging evaluation protocols. The obtained results show the superior performance of the proposed face recognition solutions adopting the novel LSTM cell architectures over ten state-of-the-art benchmarking recognition solutions.

1. Introduction

The emergence of deep neural networks as the most prominent advance in the field of pattern recognition during the past decade has enabled significantly boosting visual recognition performance [1]. Nowadays, due to their superior representation and prediction performance, deep Convolutional Neural Network (CNN) architectures are increasingly adopted for visual recognition and description [2]. CNNs take raw data as their input and extract high-level textural descriptions, using convolutional filters in multiple layers, followed by a few fully connected layers. Recurrent Neural Networks (RNNs) can be used to extract higher dimensional dependencies from sequential data, such as video or multi-view sequences, as their units have dependency connections not only between the subsequent layers, but also into themselves, to keep information from previous inputs [3]. The Long Short-Term Memory (LSTM) architecture [4] is a prominent RNN variant able to learn a model from both long- and short-term dependencies using learned gating functions. LSTM networks are widely used in many modern deep learning architectures [5], and have achieved impressive results on many large-scale learning tasks, such as speech recognition and language translation [6]. The combination of CNNs and LSTMs has recently been used for several visual recognition and description tasks, including action recognition, facial expression classification, image captioning and video description [7].

Focusing on face recognition, the application example considered in this paper, recent years have witnessed rapid advances with the development of deep learning solutions and the emergence of powerful hardware resources, like graphics processing units (GPU). Nowadays, the face recognition state-of-the-art is largely dominated by deep neural networks [8] [9] [10] [11]. However, even with the emergence of this type of sophisticated networks, certain operational conditions may still not yet allow achieving accurate enough face recognition performance. Notably, the acquired images may contain very challenging variations in the biometric data, especially in less constrained scenarios, where it is expectable to find significant variations in terms of emotions, poses, illuminations, occlusions or aging, among others [12].

Light field cameras have recently come into prominence as they are able to capture the intensity of light rays coming from multiple directions in space at a single temporal instant [13] [14]. A light field camera can ‘see’ the visual scene from different angles or perspectives, thus capturing angular variations, allowing to render the so-called *Sub-Aperture (SA) images*, corresponding to different viewpoints. The set of rendered 2D SA images can then be stored together, forming a multi-view SA array. This representation can offer *intra-view spatial* (within each view) and *inter-view angular* (across views) information, useful for various visual analysis tasks, including biometric recognition [15] [16] [17] [18] [19] and presentation attack detection [20] [21] [22] [23] [24]. Exploiting this richer spatio-angular visual representation becomes possible when using a light field camera to acquire light field images, e.g. targeting face recognition.

Recently, two deep learning based solutions [18] [19] have been proposed for light field face recognition. The first solution [18] uses the 2D-RGB central view SA image as well as its corresponding disparity and depth maps as inputs. Description creation is performed using a VGG-Face deep descriptor [25] for texture and independently fine-tuned models for the disparity and depth maps. However, these deep descriptions only correspond to the central view, ignoring the other views available in the SA multi-view array rendered from the light field. The second solution [19] proposes an end-to-end learning framework to exploit the spatio-angular information available in a light field image, creating a model which is both spatially and angularly deep, meaning it exploits both the intra-view spatial variations and the inter-view angular variations. This end-to-end learning framework includes a peephole LSTM recurrent network whose inputs are VGG-Face deep descriptions for different face viewpoints rendered from the light field image. This framework deals with angular information by organizing the SA images as a pseudo-video sequence. However, it ignores some angular dependencies and relationships, notably in terms of parallax, defined as the displacement or difference in position of an object in two images captured from different perspectives, which could be further exploited during the learning process to increase the recognition accuracy.

The main technical novelty of this paper regards the proposal of three novel LSTM cell architectures capable of jointly learning a description model by accepting as input two data sequences, simultaneously acquired, and with some dependency/relationship between them. In this paper, the two sequences represent specific horizontal and vertical SA images rendered from a single light field image, thus with a specific dependency between them related to their parallaxes; naturally, other sequences with other dependencies may be considered, implying these novel LSTM cell architectures are not limited to light field descriptions. The outcome is a learned deep model providing richer descriptions and achieving better performance for visual recognition tasks, including light field face recognition. The first LSTM cell architecture proposed adopts a *gate-level fusion* scheme, considering independent *forget*, *input*, and *output* LSTM gates for processing the two input sequences, fusing their outputs to obtain the gate-level fused output. The second architecture adopts a *state-level fusion* scheme, considering independent *cell* and *hidden* states for each input sequence, and fusing them to obtain the cell output. The last architecture adopts a *sequential learning* scheme, sequentially updating the cell state first using the information from one sequence and then from the other one, to obtain the cell output.

To show the efficiency of the novel LSTM cell architectures, they have been integrated into an end-to-end spatio-angular deep learning framework for light field based face recognition. This framework includes a LSTM network adopting the proposed LSTM cell architectures (naturally, selecting one at a time) using as inputs spatial VGG-Face deep descriptions for the horizontal and vertical SA viewpoint sequences derived from the input light field image. The learned spatio-angular descriptions, considering each of the three novel LSTM cell architectures, have been evaluated on the IST-EURECOM Light Field Face Database (LFFD) [26], which contains several facial variations, including emotions, poses, illuminations and occlusions, using three challenging evaluation protocols proposed in this paper. Results show that adopting the novel LSTM cell architectures offers more powerful light field face descriptions, able to provide significant face recognition performance improvements regarding the state-of-the-art solutions in the literature. The proposed LSTM cell architectures have also been proved to be efficient in terms of testing time, memory efficiency and parallelization ability.

The rest of the paper is organized as follows: Section 2 reviews the basic concepts of light field imaging and the long short-term memory cell architecture. The three proposed LSTM cell architectures, notably gate-level fusion, state-level fusion, and sequential learning, are presented in Section 3. Next, Section 4 reports and discusses the performance of the proposed LSTM cell architectures after integration into a deep learning framework for light field face recognition, capable of learning spatio-angular descriptions. Finally, Section 5 concludes the paper and proposes some future work.

2. Background

This section briefly reviews the basic concepts of light field imaging and the conventional LSTM cell architecture.

2.1. Light Field Imaging Basics

The proposed LSTM cell architectures deal with a new visual sensor, a *light field camera*, which allows the development of visual recognition solutions exploiting the additional visual information available, towards offering better recognition performance.

The so-called *plenoptic function*, $P(x,y,z,t,\lambda,\theta,\phi)$, was proposed in 1991 to model the information carried by the light rays at every point in the 3D space (x,y,z) , in every possible direction (θ, ϕ) , over any wavelength (λ) , and at any time (t) [27]. The so-called *static 4D light field* [28], $L(x,y,u,v)$, also known as *lumigraph* [29], was proposed in 1996, by adopting several simplifications on the plenoptic function and may be described by the intersection points of the light rays with two parallel planes [30].

There are currently two main practical setups for capturing light fields: i) a (ideally high density) array of regular (or even irregular) cameras, such as the Stanford multi-camera arrays [31] and the JPEG Pleno high density camera array (HDCA) [32]; and ii) a lenslet light field camera, using an array of micro-lenses placed in front of an image sensor to capture the light rays angular information [33]. In practice, the two acquisition approaches are rather equivalent with the main difference being the ‘camera’ baseline and all the implications in size and cost that derive from that.

A lenslet light field camera includes a digital sensor, main optics and an aperture control similar to regular cameras. The main difference regarding regular cameras comes from placing a micro-lens array on the focal plane of the main lens at a given distance from the sensor. The main lens aims to focus the light rays from the object into the microlens array. Then, the micro-lenses split the incoming light cone based on the direction of the incoming rays onto the sensor area of the corresponding micro-lens. A micro-lens array is usually composed by thousands of tiny lenses that are arranged in a rectangular, hexagonal or custom grid. In fact, each micro-lens plays the role of a small camera to acquire a so-called *micro-image* with a Bayer pattern filter [34]; Figure 1.a shows the full set of micro-images in a light field image, after color demosaicing. The micro-images can then be rendered to extract the so-called *Sub-Aperture (SA) images* corresponding to different viewpoints, thus forming a multi-view SA array which represents the visual scene. Figure 1.b and Figure 1.c show the multi-view SA array and the rendered central SA image, respectively, for the light field micro-lens image in Figure 1.a. Each 2D SA image corresponds to a slightly different viewpoint of the visual scene, meaning that a light field image captures angular information about the scene, ‘seeing’ it from different angles, which is a distinctive characteristic of this new type of visual sensor.

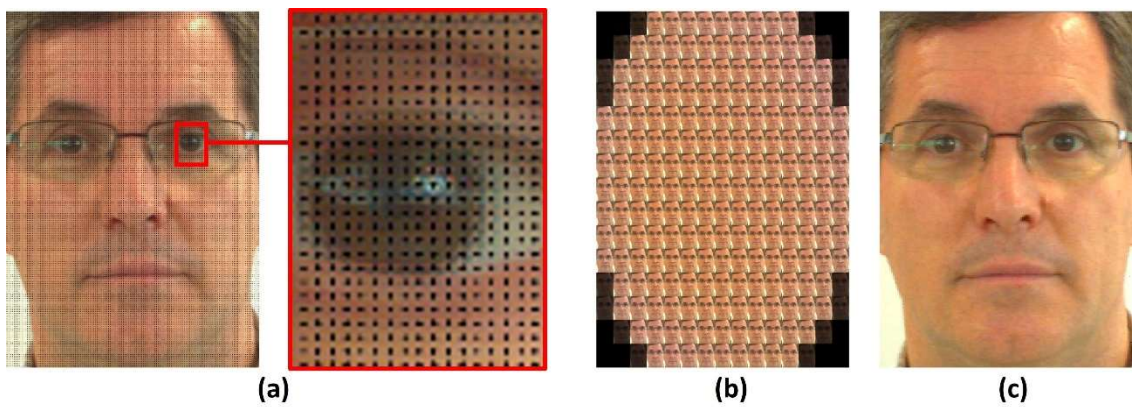


Figure 1: Light field representation: a) sample micro-images, after colour demosaicing; b) corresponding multi-view SA array; c) corresponding central SA image.

Since one light field image allows obtaining multiple 2D SA images, two types of information are available for learning: i) the intra-view, spatial information within each view; and ii) the inter-view, angular information between views, associated to the different angular capturing positions of the multiple views. It should be noted that the term ‘angular’ does not mean that angle values are processed but rather that angular dependent information/intensities are processed. The same happens when referring to ‘spatial’ information as no position coordinate values are processed but rather position dependent information/intensities are processed.

This richer spatio-angular visual representation provides a range of new capabilities to exploit/learn/describe both the intra-view, spatial information (within each view) and the inter-view, angular information (across views) for various visual recognition tasks, notably face recognition.

2.2. Long Short-Term Memory Cell Architecture

RNNs can be used to extract higher dimensional dependencies from sequential data such as video and multi-view sequences [3]. RNN units are called *cells*, and have connections not only between the subsequent layers, but also into themselves to keep information from previous inputs. The training of a RNN can be done using the *back-propagation through time* algorithm [35]. Traditional RNNs can easily learn short-term dependencies; however, they have difficulties to learn long-term dynamics as the gradients which are back-propagated can vanish or explode [36]. The Long Short-Term Memory (LSTM) is a type of RNN addressing these problems as the LSTM cells allow gradients to also flow unchanged, to avoid the gradient vanishing problem during training, while learning both long- and short-term dependencies [4] [5].

Since the introduction of LSTM in 1997 [4], the conventional LSTM (Conv-LSTM) with peephole connections has been the most commonly used cell architecture for visual recognition tasks [7]. Other variants have been proposed for different tasks such as speech recognition and language translation [5]. A LSTM network is composed by LSTM cells, whose outputs evolve throughout the network, based on past memory content. The cells have a common *cell state*, which keeps long-term dependencies along the entire LSTM cells chain, controlled by two gates, the so-called *input* and *forget* gates, thus allowing the network to decide when to forget the previous state or update the current state, given new information. The output of each cell, *hidden state*, is controlled by an *output* gate, allowing the cell to compute its output given the updated cell state. Figure 2 illustrates the Conv-LSTM cell architecture with peephole connections, which are connections from the previous cell state to the LSTM gates.

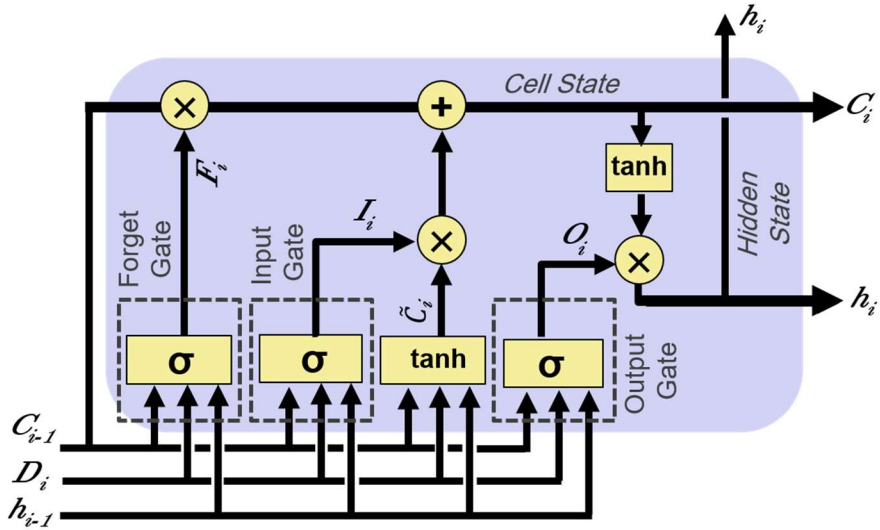


Figure 2: Architecture of a Conv-LSTM cell with peephole connections.

Each of the three gates is controlled by a sigmoid activation function, as defined by Equation 1, bounding its output to the $[0,1]$ range:

$$\sigma(x) = (1 + e^{-x})^{-1} \quad (1)$$

For a description D_i , belonging to the input description sequence, for instance deep spatial descriptions derived from images taken from a input video or multi-view sequence, the input gate output, I_i , is computed as in Equation (2), based on the input description values D_i , the previous hidden state h_{i-1} , and the previous cell state C_{i-1} (for the peephole LSTM cell architecture). The input gate learns how to add information to the cell state.

$$I_i = \sigma(W_I[D_i + h_{i-1} + C_{i-1}] + b_I) \quad (2)$$

where W_I is the input gate weight and b_I is the input gate bias.

Equation (3) creates new cell state candidate values, \tilde{C}_i , that may be added to the cell state later:

$$\tilde{C}_i = \tanh(W_{\tilde{C}}[D_i + h_{i-1} + C_{i-1}] + b_{\tilde{C}}) \quad (3)$$

where $W_{\tilde{C}}$ is the new candidate values weights and $b_{\tilde{C}}$ is the new candidate values biases. The hyperbolic tangent activation function, \tanh , is the nonlinearity function used for creating the candidate values, \tilde{C}_i , defined as:

$$\tanh(x) = 2\sigma(2x) - 1 \quad (4)$$

The forget gate, F_i , learns how to forget information from the cell state, according to:

$$F_i = \sigma(W_F[D_i + h_{i-1} + C_{i-1}] + b_F) \quad (5)$$

where W_F is the forget gate weight and b_F is the forget gate bias.

Then, based on I_i , F_i , and \tilde{C}_i , the previous cell state, C_{i-1} , is updated to obtain C_i as follows:

$$C_i = F_i \odot C_{i-1} + I_i \odot \tilde{C}_i \quad (6)$$

where \odot denotes the vector element-wise product. As the output values for I_i and F_i lie in the range $[0,1]$, the LSTM selectively learns to consider or forget the current input and the previous state.

The current cell state, C_i , can then be used for predicting the current cell's hidden state, h_i , according to Equations (7) and (8), thus allowing the LSTM to learn how much from the cell memory should be included into the hidden state:

$$O_i = \sigma(W_O[D_i + h_{i-1} + C_{i-1}] + b_O) \quad (7)$$

$$h_i = O_i \odot \tanh(C_i) \quad (8)$$

where W_O is the output gate weight and b_O is the output gate bias.

The hidden state, h_i , is the cell output for the input description D_i . The hidden state is taken as input by the next LSTM cell in the LSTM network architecture, as illustrated in Figure 3. The number of cells in a LSTM network equals the number of inputs, e.g. images/descriptions in the input sequence. The output of each LSTM cell corresponds to a description produced by taking into account the short- and long-term dependencies observed up to that cell's input image/description.

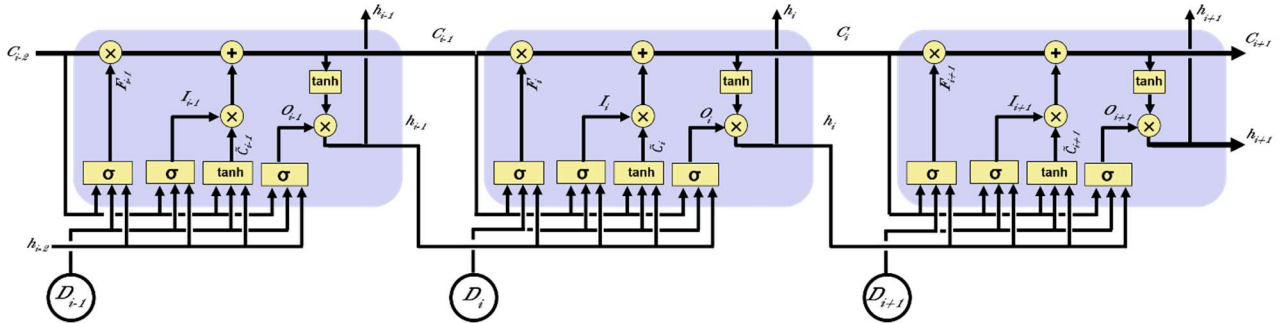


Figure 3: A LSTM network composed by several conventional LSTM cells.

3. Proposed Long Short-Term Memory Cell Architectures

A conventional LSTM network can learn a model to describe the information coming from one input sequence, e.g. of 2D images or descriptions. However, if two dependent sequences of data are simultaneously acquired with some specific dependency, the conventional LSTM cell architecture may only process these sequences sequentially, thus not taking benefit of the information carried out by the dependencies. In this context, novel LSTM cell architectures may be designed to jointly learn from those two sequences. The term *joint learning* implies that the each of the proposed novel LSTM cell architectures should simultaneously receive two sequences as input, such as sequences of horizontal and vertical SA views rendered from a light field image, which have a specific dependency associated to their parallax. A more expressive deep model can then be learned by simultaneously processing both input sequences, creating richer descriptions for visual recognition tasks [19].

In this context, this paper proposes three novel LSTM cell architectures able to jointly learn from two input sequences, and not just from a single input sequence as the Conv-LSTM, to create more discriminative descriptions for visual recognition tasks. In this paper, light field face recognition is adopted as the target

application, to demonstrate the added value of the novel LSTM cell architectures. The horizontal and vertical parallaxes (see Figure 4), defined as the displacement or difference in position of an object in two images captured from different perspectives, e.g., horizontal or vertical, can represent the viewpoint changes captured in a light field image as discussed in [19], thus defining the two LSTM cell input sequences to consider.

The Conv-LSTM cell architecture can learn the horizontal or the vertical inter-view angular information, as it accepts a single sequence as its input. In order to capture both the horizontal and vertical angular variations, one possibility is to scan the horizontal SA images followed by the vertical ones, thus creating a single pseudo-video sequence to be used as the LSTM network input. However, this *sequential concatenation* implies a viewpoint description discontinuity when moving from the last horizontal SA image position to the first vertical one, which may lead to a degraded learning performance [19]. Additionally, by dealing with the inter-view horizontal and vertical angular information as a single merged pseudo-video sequence, or as two independent pseudo-video sequences, some additional dependencies between the horizontal and vertical angular information may be ignored, such as the parallax relations, that could be further exploited during the learning process to increase the recognition accuracy.

To jointly learn the inter-view angular information along the horizontal and vertical directions for light field face recognition, each novel LSTM cell receives two input sequences. As a consequence, an LSTM network built with the novel LSTM cell architectures requires half the number of cells, when compared to an LSTM network with the conventional LSTM cells, since each cell now analyzes two inputs at once. In the considered light field example, the first LSTM cell in the LSTM network receives its two inputs from the most left and top SA images, in the middle row and middle column, respectively, as highlighted by the blue boxes in Figure 4. The second LSTM cell processes the second most left and the second top SA images from the middle row and the middle column, respectively, and so on. With the new LSTM cell architectures, this relationship may be also jointly exploited.

In the considered light field face recognition framework, SA images are not directly processed by the LSTM network. In fact, it is common practice [7] to first extract spatial descriptions from each input SA image, to first learn from the intra-view spatial information, and then use the LSTM network to also learn the inter-view angular information from the spatial description input sequences. In the present proposal, a single light field image is analyzed, and thus pseudo-video sequences are created using selected sets of SA images from the multi-view SA array. A deep CNN is used to extract intra-view spatial description sequences, which are then passed to the novel LSTM architectures. Naturally, other descriptors for the intra-view spatial information could be also considered.

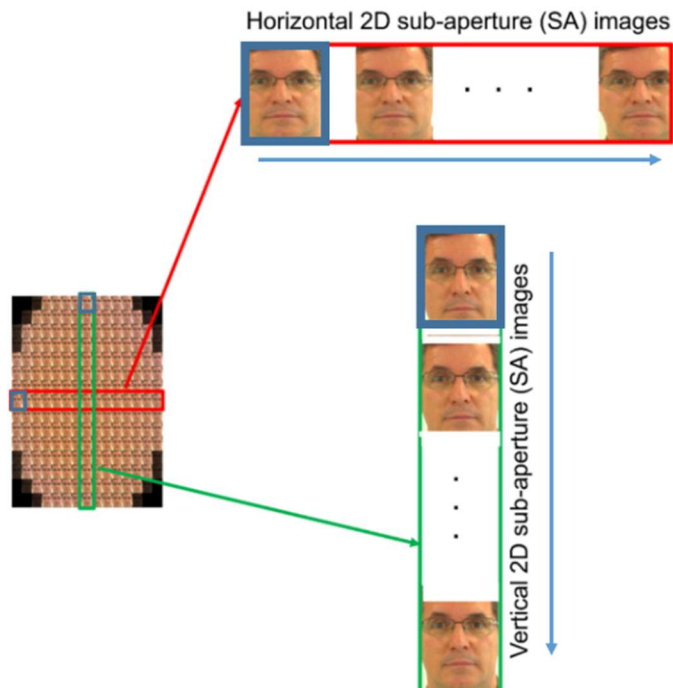


Figure 4: Multi-view array of SA face images and the selected set of horizontal and vertical 2D SA images, corresponding to slightly different viewpoints.

The proposed LSTM cell architectures considering *gate-level fusion*, *state-level fusion*, and *sequential learning* schemes, are described in the following. For better understanding, and since the novel LSTM cell architectures will be later used for light field face recognition, the two input sequences to the novel LSTM cell architectures will be named as horizontal, Hi , and vertical, Vi , spatial descriptions, corresponding to the application considered in Section 4. However, the novel LSTM cell architectures may also consider other types of input sequences with other dependencies, addressing other analysis tasks.

3.1. Gate-Level Fusion LSTM (GLF-LSTM) Cell Architecture

The first proposed LSTM cell architecture adopts a *gate-level fusion* scheme, separately learning the horizontal and vertical forget, input and output gates and then merging the horizontal and vertical gates' outputs to compute the fused gates' output. In this context, the cell and hidden state outputs are controlled by the fused gates, thus providing richer joint information to learn a model from the light field angular information.

As illustrated in Figure 5, the horizontal, HI_i , and vertical, VI_i , input gates are computed according to Equations (9) and (10), respectively, independently learning how to add horizontal and vertical information to the cell state. The horizontal and vertical input gates can be computed for view number i , based on the spatial descriptions Hi and Vi , respectively extracted from the horizontal and vertical multi-view description sequences, the previous hidden state h_{i-1} , and the previous cell state C_{i-1} as:

$$HI_i = \sigma(W_{HI}[Hi + h_{i-1} + C_{i-1}] + b_{HI}) \quad (9)$$

$$VI_i = \sigma(W_{VI}[Vi + h_{i-1} + C_{i-1}] + b_{VI}) \quad (10)$$

where W_{HI} and W_{VI} are the horizontal and vertical input gates weights, respectively, and b_{HI} and b_{VI} are the horizontal and vertical input gates bias, respectively.

Then, the fused input gate, I_i , is computed by adding the horizontal and vertical input gates together:

$$I_i = [HI_i + VI_i] \quad (11)$$

The horizontal, \widetilde{HC}_i , and vertical \widetilde{VC}_i , candidate values are computed according to Equations (12) and (13), respectively, thus deciding about the horizontal and vertical information that may be added to the cell state later. Horizontal and vertical candidate values are then fused to compute the fused candidate value, \tilde{C}_i , (Equation (14)):

$$\widetilde{HC}_i = \tanh(W_{\widetilde{HC}}[Hi + h_{i-1} + C_{i-1}] + b_{\widetilde{HC}}) \quad (12)$$

$$\widetilde{VC}_i = \tanh(W_{\widetilde{VC}}[Vi + h_{i-1} + C_{i-1}] + b_{\widetilde{VC}}) \quad (13)$$

$$\tilde{C}_i = [\widetilde{HC}_i + \widetilde{VC}_i] \quad (14)$$

where $W_{\widetilde{HC}}$ and $W_{\widetilde{VC}}$ are the horizontal and vertical candidate values weights, respectively, and $b_{\widetilde{HC}}$ and $b_{\widetilde{VC}}$ are the horizontal and vertical candidate values biases, respectively.

Next, the horizontal, HF_i , and vertical, VF_i , forget gates are computed according to Equations (15) and (16), respectively, learning how to forget horizontal and vertical information from the cell state, and then are fused to compute the fused hidden state, \tilde{C}_i , (Equation (17)).

$$HF_i = \sigma(W_{HF}[Hi + h_{i-1} + C_{i-1}] + b_{HF}) \quad (15)$$

$$VF_i = \sigma(W_{VF}[Vi + h_{i-1} + C_{i-1}] + b_{VF}) \quad (16)$$

$$F_i = [HF_i + VF_i] \quad (17)$$

where W_{HF} and W_{VF} are the horizontal and vertical forget gates weights, respectively, and b_{HF} and b_{VF} are the horizontal and vertical forget gates biases, respectively.

Then, based on I_i , F_i , and \tilde{C}_i , the previous cell state, C_{i-1} , is updated to obtain C_i , according to Equations (18), to update the long-term memory observed so far with respect to the horizontal and vertical information observed in the current horizontal and vertical view descriptions:

$$C_i = F_i \odot C_{i-1} + I_i \odot \tilde{C}_i \quad (18)$$

The horizontal, HO_i , and vertical, VO_i , output gates are computed according to Equations (19) and (20), respectively, learning how to update hidden state, and then are added to compute the fused output gate, O_i , according to Equation (21).

$$HO_i = \sigma(W_{HO}[H_i + h_{i-1} + C_{i-1}] + b_{HO}) \quad (19)$$

$$VO_i = \sigma(W_{VO}[V_i + h_{i-1} + C_{i-1}] + b_{VO}) \quad (20)$$

$$O_i = [HO_i + VO_i] \quad (21)$$

where W_{HO} and W_{VO} are the horizontal and vertical output gates weights, respectively, and b_{HO} and b_{VO} are the horizontal and vertical input gates biases, respectively.

The current cell state, C_i , already updated with respect to the jointly learned fused gates and the fused output gate, O_i , can then be used for predicting the current cell's hidden state, h_i , according to Equation (22), thus producing the final description for the GLF-LSTM cell:

$$h_i = O_i \odot \tanh(C_i) \quad (22)$$

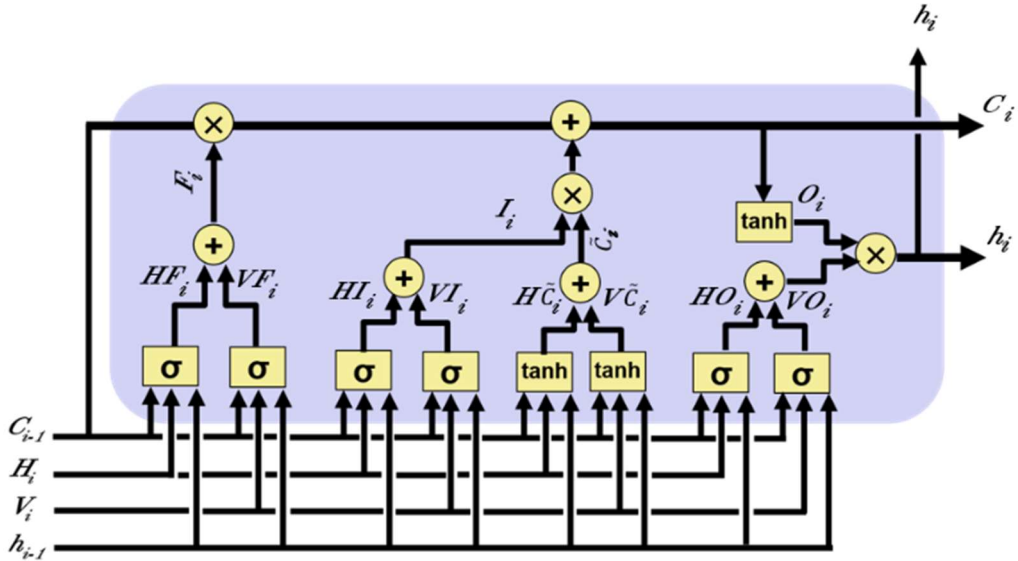


Figure 5: Proposed GLF-LSTM cell architecture.

The GLF-LSTM cell architecture jointly learns a deep model from light field horizontal and vertical information, in the form of *fused gates*, composed by independent horizontal and vertical gates. The computation of the horizontal and vertical input, forget, and output gates can be done in parallel, as the learning of W_{HI} , W_{VI} , $W_{\tilde{C}}$, and W_{HO} horizontal weights is independent from that of W_{VI} , W_{VI} , $W_{\tilde{C}}$, and W_{VO} vertical weights. Although this independency increases parallelism and, thus, may reduce the computational time, it implies that the vertical and horizontal gates cannot establish a learning interaction between themselves when optimizing learning weights for updating the cell state.

3.2. State-Level Fusion LSTM (SLF-LSTM) Cell Architecture

The second proposed LSTM cell architecture provides a *state-level fusion* scheme, separately learning the horizontal and vertical cell and hidden states, and then merging the horizontal and vertical states outputs to compute the fused cell and hidden state outputs.

As illustrated in Figure 6, first, the horizontal elements, including horizontal input gate (Equation (23)), candidate list (Equation (24)), and forget gate (Equation (25)), are computed based on the horizontal view description Hi , the previous hidden state h_{i-1} , and the previous cell state C_{i-1} :

$$HI_i = \sigma(W_{HI}[H_i + h_{i-1} + C_{i-1}] + b_{HI}) \quad (23)$$

$$\tilde{H}C_i = \tanh(W_{\tilde{H}C}[H_i + h_{i-1} + C_{i-1}] + b_{\tilde{H}C}) \quad (24)$$

$$HF_i = \sigma(W_{HF}[H_i + h_{i-1} + C_{i-1}] + b_{HF}) \quad (25)$$

Then, based on HI_i , HF_i , and \widetilde{HC}_i , the previous cell state, C_{i-1} , is updated to obtain horizontal cell state HC_i , according to Equation (26). This means the long-term memory, including horizontal and vertical information observed so far, is updated with respect to the horizontal information observed in the current view description:

$$HC_i = HF_i \odot HC_{i-1} + HI_i \odot H \widetilde{C}_i \quad (26)$$

To learn how to update horizontal hidden state, the horizontal output gate, HO_i , is computed as:

$$HO_i = \sigma(W_{HO}[H_i + h_{i-1} + C_{i-1}] + b_{HO}) \quad (27)$$

The horizontal cell state, HC_i , already updated with respect to the horizontal gates, along with the horizontal output gate, can be used for predicting the horizontal cell's hidden state, Hh_i , according to Equation (28), thus producing the horizontal description for the SLF-LSTM cell:

$$Hh_i = HO_i \odot \tanh(HC_i) \quad (28)$$

Next, the vertical elements, including vertical input gate (VI_i), candidate list (\widetilde{VC}_i), forget gate (VF_i), cell state (VC_i), output gate (VO_i), and hidden state (Vh_i) are computed, according to Equations (29), (30), (31), (32), (33), and (34), respectively, based on the vertical spatial description V_i , the previous hidden state h_{i-1} , and the previous cell state C_{i-1} :

$$VI_i = \sigma(W_{VI}[V_i + h_{i-1} + C_{i-1}] + b_{VI}) \quad (29)$$

$$\widetilde{VC}_i = \tanh(W_{VC}[V_i + h_{i-1} + C_{i-1}] + b_{VC}) \quad (30)$$

$$VF_i = \sigma(W_{VF}[V_i + h_{i-1} + C_{i-1}] + b_{VF}) \quad (31)$$

$$VC_i = VF_i \odot VC_{i-1} + VI_i \odot \widetilde{VC}_i \quad (32)$$

$$VO_i = \sigma(W_{VO}[V_i + h_{i-1} + C_{i-1}] + b_{VO}) \quad (33)$$

$$Vh_i = VO_i \odot \tanh(VC_i) \quad (34)$$

Finally, the cell and hidden state outputs, that were independently computed based on horizontal and vertical information, are added together to compute the fused cell state, C_i , and the fused hidden state, h_i , according to:

$$C_i = [HC_i + VC_i] \quad (35)$$

$$h_i = [Hh_i + Vh_i] \quad (36)$$

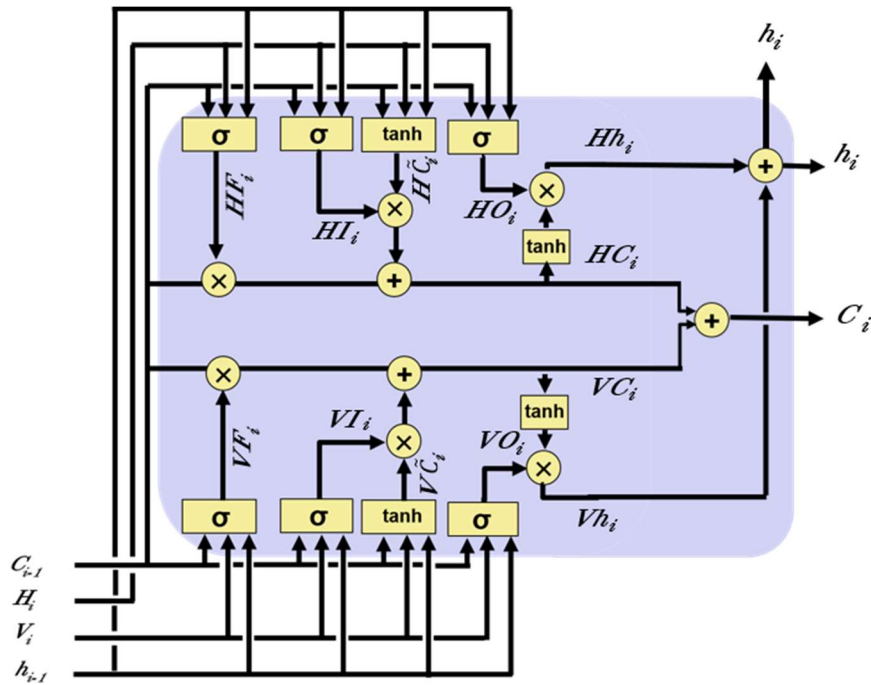


Figure 6: Proposed SLF-LSTM cell architecture.

The SLF-LSTM cell architecture jointly learns a model from the light field horizontal and vertical information, in the form of *fused states* composed by independent, horizontal and vertical states. The SLF-LSTM parallelism capability is the same as for GLF-LSTM since all the horizontal and vertical learning weights are independently computed. The SLF-LSTM architecture implies not only that vertical and horizontal gates cannot establish a learning interaction between themselves, but the fused horizontal and vertical gates also cannot do so when optimizing the learning weights for updating the cell and hidden states either, which may reduce the learning efficiency.

3.3. Sequential Learning LSTM (SeqL-LSTM) Cell Architecture

The last proposed light field cell architecture performs *sequential learning* by modeling in sequence the angular information available in the horizontal and vertical parallaxes. Unlike the previous cell architecture proposals, in this approach, the cell state is not updated based on fusion schemes.

The SeqL-LSTM cell architecture cell is illustrated in Figure 7. Horizontal input gate (Equation (37)), candidate list (Equation (38)), and forget gate (Equation (39)) are, respectively, computed based on the horizontal spatial description H_i , the previous hidden state h_{i-1} , and the previous cell state C_{i-1} :

$$HI_i = \sigma(W_{HI}[H_i + h_{i-1} + C_{i-1}] + b_{HI}) \quad (37)$$

$$\widetilde{HC}_i = \tanh(W_{\widetilde{HC}}[H_i + h_{i-1} + C_{i-1}] + b_{\widetilde{HC}}) \quad (38)$$

$$HF_i = \sigma(W_{HF}[H_i + h_{i-1} + C_{i-1}] + b_{HF}) \quad (39)$$

The proposed cell architecture updates the cell state, i.e., long-term memory, using horizontal information observed in the current view description according to Equation (40):

$$HC_i = HF_i \odot C_{i-1} + HI_i \odot \widetilde{HC}_i \quad (40)$$

In this context, the cell state expresses the previous horizontal and vertical information observed in previous view descriptions, as well as the horizontal information observed in the current view description. Then, the vertical input gate (Equation (41)), candidate list (Equation (42)), and forget gate (Equation (43)) are computed based on the vertical spatial description V_i , the previous hidden state h_{i-1} , and the previous cell state C_{i-1} :

$$VI_i = \sigma(W_{VI}[V_i + h_{i-1} + C_{i-1}] + b_{VI}) \quad (41)$$

$$\widetilde{VC}_i = \tanh(W_{\widetilde{VC}}[V_i + h_{i-1} + C_{i-1}] + b_{\widetilde{VC}}) \quad (42)$$

$$VF_i = \sigma(W_{VF}[V_i + h_{i-1} + C_{i-1}] + b_{VF}) \quad (43)$$

Based on Equation (40), the cell state is already learned from the horizontal and vertical information observed in previous views descriptions and the horizontal information observed in the current view description. In the next step, the cell state is updated according to Equation (44), thus sequentially updating the cell state with the vertical information observed in the current view description.

$$C_i = VF_i \odot HC_i + VI_i \odot \widetilde{VC}_i \quad (44)$$

The horizontal, HO_i , and vertical, VO_i , output gates are computed according to Equations (45) and (46), respectively, learning how to update the hidden state:

$$HO_i = \sigma(W_{HO}[H_i + h_{i-1} + C_{i-1}] + b_{HO}) \quad (45)$$

$$VO_i = \sigma(W_{VO}[V_i + h_{i-1} + C_{i-1}] + b_{VO}) \quad (46)$$

Finally, based on the sequentially learned cell state, the vertical hidden state, Vh_i , and the horizontal hidden state, Hh_i , are computed, according to Equations (47) and (48), respectively, and then are added to compute the fused hidden state, H_i , according to Equation (49), providing the final SeqL-LSTM description:

$$Vh_i = HO_i \odot \tanh(C_i) \quad (47)$$

$$Hh_i = VO_i \odot \tanh(C_i) \quad (48)$$

$$h_i = [Hh_i + Vh_i] \quad (49)$$

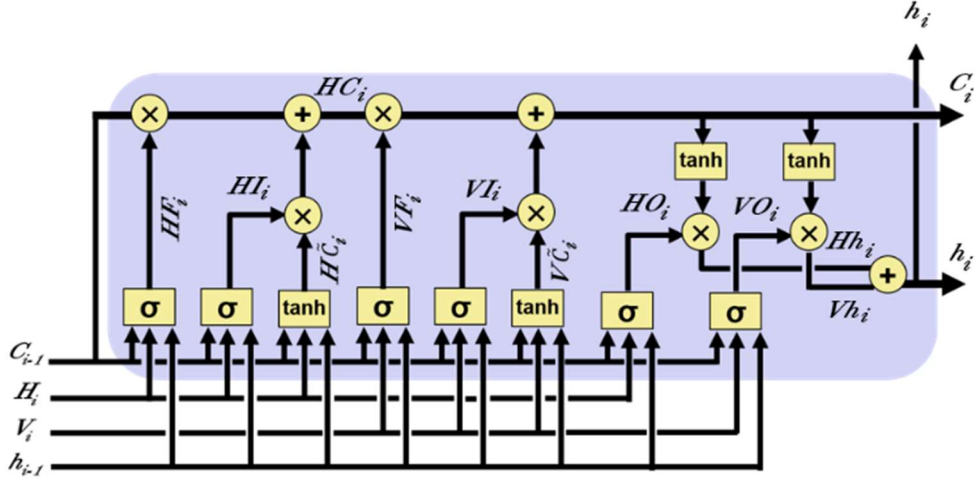


Figure 7: Proposed SeqL-LSTM cell architecture.

The SeqL-LSTM cell architecture establishes a learning interaction between the horizontal and vertical input, forget and candidate value weights when updating the cell state, which is expected to provide a better learning and, thus, a better angular description than the SLF-LSTM and GLF-LSTM cell architectures since their limitations are at least partly overcome. Indeed, the vertical weights are optimized considering the fact that the horizontal information for the current input has already been observed, and thus the horizontal weights for updating the cell state are already optimized, which is not the case for the other two proposed LSTM cell architectures. However, the expected superior SeqL-LSTM cell architecture performance comes at the cost of reducing the parallelization ability, as updating the SeqL-LSTM cell state must be done in a serial way.

4. Application of the Novel LSTM Cell Architectures to Light Field Face Recognition

The three proposed LSTM cell architectures have been integrated into a spatio-angular deep learning framework for light field face recognition. This section presents the recognition framework architecture, test material and protocols, state-of-the-art benchmarking solutions, and performance assessment, in terms of recognition accuracy, computational complexity, memory efficiency, and parallelization ability.

4.1. Architecture and Walkthrough

The three proposed LSTM cell architectures have been integrated (naturally, one at a time) into a spatio-angular deep learning framework for face recognition, whose inputs come from a VGG-Face deep descriptor applied to a selected set of 2D horizontal and vertical SA face image sequences derived from a light field image. The differences between the proposed spatio-angular deep learning framework in this paper and the one used in [19], adopting Conv-LSTM cells, are twofold: i) the Conv-LSTM cell architecture used in [19] is replaced by the new LSTM cell architectures proposed in this paper; and ii) while in [19] different methods are considered to select the one sequence of representative SA images, notably varying in their number, position and scanning order, this paper selects two sequences, corresponding to the middle row and the middle column SA images, as they can represent the essential light field information coming from multiple directions, notably with maximum parallax [19].

The architecture of the proposed spatio-angular description framework for face recognition is presented in Figure 8. It should be noted that the three proposed LSTM cell architectures lead to three different recognition solutions to model the views spatio-angular information. The framework includes the main modules described in the following.

1. Pre-processing: First, the light field raw (LFR) input image is rendered using the Light Field Toolbox v0.4 software [38], to create the multi-view SA array, which includes 15×15 SA images, each with a spatial resolution of 625×434 pixels. Then, the face region within each SA image is cropped and resized to 224×224 pixels, which is the expected input size for the VGG-Face descriptor.

2. Horizontal and vertical SA image selection: This module independently scans the middle row and the middle column SA images into two SA image pseudo-video view sequences, each including fifteen SA images (the usual reduction to 13 SA images is not needed as the vignetting effect is not strong for the middle row and column). These images represent viewpoint changes along the horizontal and vertical

directions with maximum parallax, thus expected to capture the light field information coming from multiple directions.

3. VGG-Face spatial description: Each selected SA image is fed to a *pre-trained* VGG-Very-Deep-16 CNN architecture [37], to extract a VGG-Face description with a fixed length of 4096 elements. This work uses the pre-trained VGG-Face model [25], highlighted in dark yellow in Figure 8, with no additional training being performed at this stage. It should be noted that the training of the VGG-Face model was done with totally different content [25] from the test material used in this paper.

4. LSTM spatio-angular description: During the training, the created horizontal and vertical intra-view spatial VGG-Face description sequences are provided to one of the proposed LSTM cell architectures, which jointly learn from them to train the deep spatio-angular LSTM model. The LSTM network model, highlighted in purple in Figure 8, is then used to create deep spatio-angular descriptions from the sequences of SA view descriptions. Naturally, the number of LSTM cells in a LSTM network equals the number of views in the horizontal or vertical input view sequences. The SeqL-LSTM cell architecture has been used in Figure 8 for illustration purposes.

5. Softmax classification: The set of LSTM cell outputs, corresponding to the short- and long-term inter-view angular dependencies, are used as input to a softmax classifier. A classification model is learned during training, so that at test time the deep spatio-angular descriptions created can be used to recognize the identity of the person in the input light field image, using the classification model. In order to consider all LSTM hidden states, each corresponding to an input light field view description, their average is calculated, and then compared to the classification model for recognition purposes [7] [19].

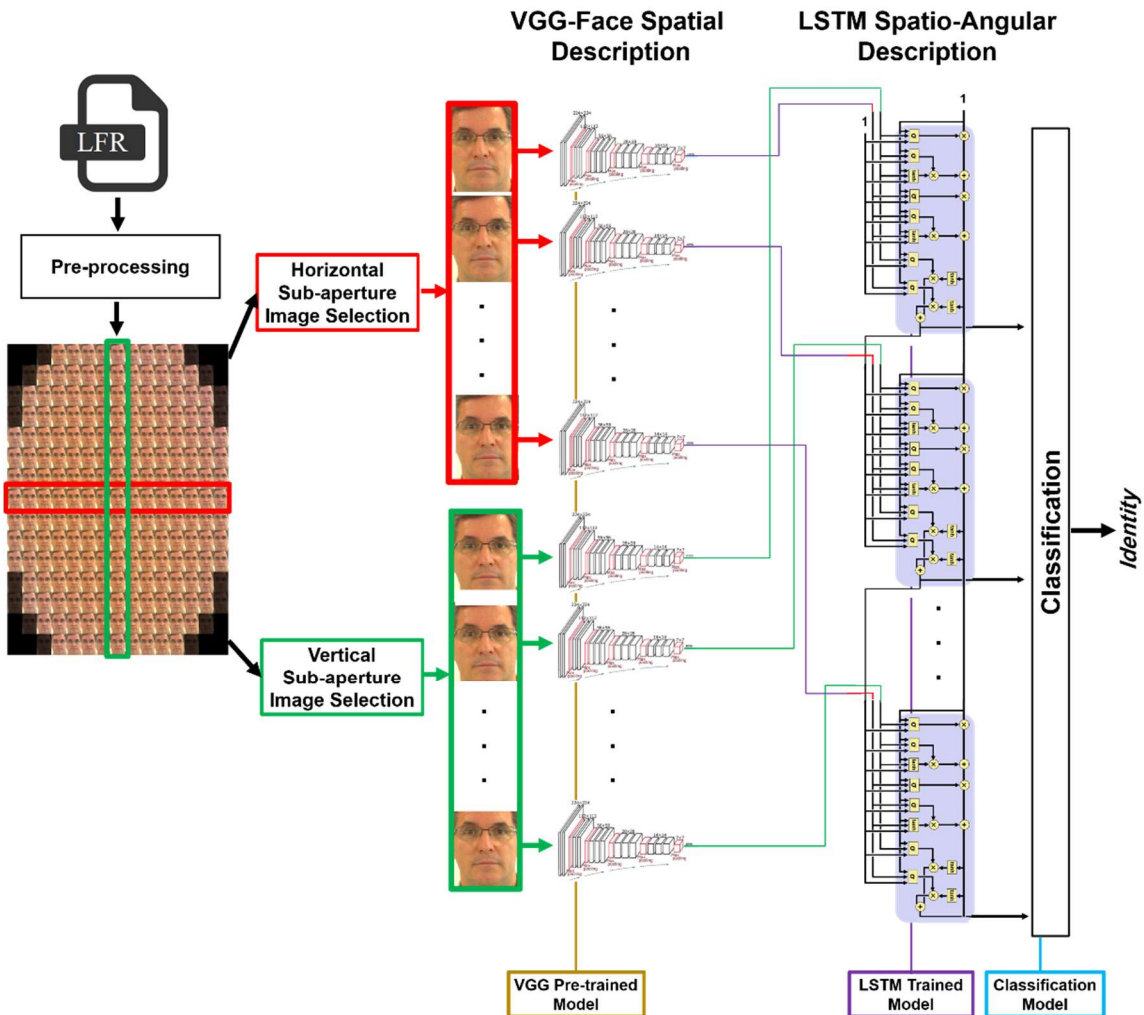


Figure 8: Architecture of the spatio-angular based learning framework for light field face recognition when adopting SeqL-LSTM cells.

In summary, the adoption of the proposed LSTM cell architectures in the context of a spatio-angular recognition framework offers very powerful solutions, by exploiting both the intra-view spatial and combined horizontal and the

vertical inter-view angular information available in light field images, leading to a boost in face recognition performance.

4.2. Test material and protocols

The IST-EURECOM Light Field Face Database (LFFD) [26], consisting of light field face images captured by a Lytro ILLUM camera [39], is used in this work for performance assessment purposes. IST-EURECOM LFFD includes 4000 light field images, captured from 100 subjects in two separate acquisition sessions, with a temporal separation between 1 and 6 months. Each session contains 20 light field images per subject with different facial variations including facial emotions, actions, poses, illuminations and occlusions, as illustrated in Figure 9, thus defining different face recognition tasks.



Figure 9: IST EURECOM LFFD: Illustration of 2D central SA cropped images from one acquisition session.

This paper proposes three test protocols with practical meaningfulness to assess the performance of the proposed LSTM cell architectures in the context of the face recognition framework described in Section 4. The test protocols are defined as follows:

- **Protocol 1:** The training set contains only the neutral light field images from the first acquisition session (1 image per subject), while the validation set includes the left and right half-profile images from the same acquisition session (2 images per subject), thus corresponding to a low-complexity enrolment and training scenario; the testing set includes all the light field images from the second acquisition session, as illustrated in Figure 10.a. This '*single training image per person*' protocol is the simplest protocol considered, but it is the most challenging in terms of recognition performance as training is poor/simple in terms of used information.
- **Protocol 2:** The training set contains the neutral plus the left and right full-profile light field images from the first acquisition session (3 images per subject), while the testing set includes all the light field images from the second acquisition session, as illustrated in Figure 10.b. The validation set includes the left and right half-profile images from the same (first) acquisition session (2 images per subject). This protocol also assumes a rather simple and quick enrolment phase thus corresponding to a low-complexity enrolment and training scenario and is slightly less challenging than the first protocol in terms of recognition performance because information is used for the training.
- **Protocol 3:** The training set contains all twenty database face variations captured during the first acquisition session, while the validation and testing sets each consider half of the second session images, as illustrated in Figure 10.c, thus corresponding to a higher-complexity enrolment and training scenario. This scenario is less challenging in terms of recognition performance as the system learns more in the training phase.

The first and second protocols (*Protocol 1* and *Protocol 2*) correspond to application scenario where each person registers/enrolls into the system by quickly taking just one or three photos in a controlled setup, similar to the famous police station paradigm. Testing is done by considering all facial variations captured in the second acquisition session, assuming that the recognition should be robust to real-life conditions where the face images to be used for recognition may have captured in less constrained conditions, notably including facial expressions or be partly occluded, for instance. With these protocols, the recognition system has not been exposed/trained with many of the facial variations with which it will be tested.

The third protocol (*Protocol 3*) assumes a more complex acquisition phase, considering more training images, under the assumption that the increased complexity will result in a better trained and thus more knowledgeable overall model, which should offer a better recognition performance. This protocol divides the available database material into disjoint training (50%), validation (25%), and testing (25%) sets, where the first session light field images are all used for training. In this case, the recognition system has been initially exposed/trained to more facial variations, increasing the initial complexity to get better description and classification models, and thus achieve a better recognition performance.

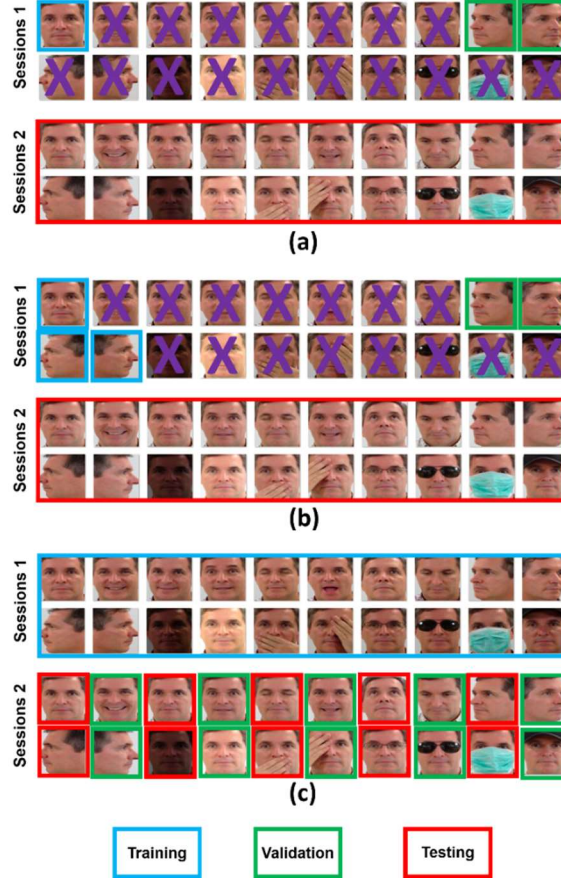


Figure 10: IST-EURECOM LFFD database division into training, validation and testing sets (a) Protocol 1; (b) Protocol 2; and (c) Protocol 3.

The three protocols correspond to *cooperative user scenarios*, offering different trade-offs in terms of the initial enrolment and training complexity versus the expected recognition performance. The first and second protocols have multiple practical applications, such as access control systems, where the users can be registered/enrolled into the system by quickly taking a mugshot, including a frontal-view and side-view photos in a controlled setup. Then, the goal is to recognize a person from an image captured at a different time, and possibly in non-ideal conditions, e.g. exhibiting unpredictable facial variations. The third protocol corresponds to a more cooperative user scenario, targeting applications with increased security requirements, where the users are willing to cooperate more during the registration phase, simulating different facial variations, over a range of expressions, actions, poses, illuminations, and occlusions, to capture as many variations as possible during the enrollment phase, so that the proposed recognition system can more effectively recognize users during the daily operation of the system.

4.3. Benchmarking Recognition Solutions

The three proposed LSTM cell architectures lead to three recognition solutions when adopted in the proposed face recognition framework. These solutions are labelled as GLF-LSTM, SLF-LSTM and SeqL-LSTM and are variations of the initial Conv-LSTM recognition solution when the LSTM cell architecture changes.

The alternative recognition solutions considered for benchmarking purposes are grouped into two categories:

1. **2D based solutions**, including Principle Component Analysis (PCA) [40], Histogram of Oriented Gradients (HOG) [41], Local Binary Patterns (LBP) [42], and VGG-Face [25], which process only the (single) central SA image;
2. **Light field based solutions**, including fused light field deep representation [18], Depth Local Binary Patterns (DLBP) [43], Light Field Local Binary Patterns (LFLBP) [16], HOG+Histogram of Disparity Gradients (HDG) [17], Multi-linear Principle Component Analysis (MPCA) [44], VGG 2D+Disparity+Depth (VGG-D³) [18], VGG+conventional LSTM [19], which process different types and amounts of the light field image data.

It should be noted that all tested recognition solutions were re-implemented by the authors of this paper for the proposed test protocols and performance results were obtained considering the best parameter settings reported in the relevant original papers. For the relevant solutions, the disparity maps have been obtained using the methods proposed in [45] and [46], and the depth maps have been obtained using the method proposed in [47] for [43] [18].

4.4. Hyper-Parameters Selection

The recognition performance sensitivity to the LSTM hyper-parameter setting, notably hidden layer size, training batch size and number of epochs to consider for network convergence, has been studied using the validation sets with the target of tuning the LSTM model hyper-parameters. The validation results showed that the best performance for the proposed LSTM cell architectures is achieved when setting the hidden layer size to 256, the training batch size to 100 and 500 training epochs are used. This hyper-parameters configuration has been used for the final recognition accuracy performance assessment.

4.5. Comparative Recognition Accuracy

Tables 1, 2, and 3 report the rank-1 recognition rates obtained, respectively, for test protocols 1, 2, and 3, for the proposed recognition solutions and the 10 selected benchmarking solutions. The results in these tables are presented for the five recognition tasks corresponding to the LFFD dimensions (shown in Figure 9), notably emotions, actions, poses, illuminations and occlusions, using all the test set images as defined for each test protocols presented above; the best results are highlighted in bold.

Comparison with 2D based solutions: The results clearly show that all the recognition solutions adopting the proposed LSTM cell architectures perform significantly better than all non-deep learning based 2D based recognition solutions, including, PCA [40], HOG [41] and LBP [42]. Moreover all the proposed solutions achieve average performance gains larger than 10% when compared to the baseline 2D VGG-face descriptor that creates deep spatial descriptions only for the central SA image [25].

Comparison with light field based solutions: The obtained rank-1 recognition results demonstrate the superiority of the proposed solutions when compared to the non-deep learning light field based solutions, including MPCA [44], DLBP [43], LFLBP [16] and HOG+HDG [17]. The results also show that the recognition solutions adopting the proposed LSTM cell architectures achieve better performance than VGG-D³ [18] for all face recognition tasks considered. The results clearly show the superiority of the three proposed recognition solutions based on the three proposed LSTM cell architectures over the best performing benchmarking solution, the Conv-LSTM solution, for almost all the face recognition tasks considered. The added value of the proposed LSTM cell architectures is more evident for the more challenging tasks, notably pose variations and occlusions, where the new joint learning from the light field horizontal and vertical view descriptions, leading to richer spatio-angular descriptions, contributes to improve the final recognition performance. Additionally, this superiority is more evident for the protocols with limited amounts of training data, i.e., protocols 1 and 2, what again highlight the increased efficiency of the proposed solutions.

Comparison of the proposed LSTM cell architectures: Finally, the performance results show that the proposed VGG+SeqL-LSTM recognition solution works slightly better than the other proposed solutions based on the other proposed LSTM cell architectures, i.e. VGG+GLF-LSTM and VGG+SLF-LSTM, due to establishing a learning interaction between vertical and horizontal weights, when updating the cell state, thus proving a better inter-view angular description.

Table 1: Protocol 1 assessment: Face recognition rank-1 for the proposed and benchmarking recognition solutions (proposed solutions and best results in bold).

Face recognition solution		Recognition Tasks					
		Neutral & emotion	Action	Pose	Illumination	Occlusion	Average
Name	Type						
PCA [40]	2D	28.50%	28.00%	06.67%	12.50%	16.33%	17.40%
LBP [42]	2D	16.75%	18.50%	06.67%	12.00%	09.33%	11.20%
HOG [41]	2D	57.50%	58.50%	09.83%	48.00%	38.33%	36.60%
VGG-Face [25]	2D	99.50%	99.00%	56.33%	99.00%	74.67%	79.00%
DLBP [43]	LF	59.25%	64.50%	30.33%	24.50%	22.33%	36.55%
MPCA [44]	LF	36.75%	33.50%	07.50%	14.50%	19.67%	20.30%
LFLBP [16]	LF	34.25%	31.00%	10.17%	17.00%	13.17%	18.65%
HOG+HDG [17]	LF	62.25%	62.50%	12.00%	62.00%	41.33%	40.90%
VGG-D ³ [18]	LF	99.50%	99.00%	56.50%	99.00%	75.50%	79.50%
VGG + Conv-LSTM [19]	LF	99.25%	99.50%	71.67%	99.00%	91.17%	88.55%
Prop. VGG + GLF-LSTM	LF	99.50%	100%	71.33%	99.00%	92.00%	88.75%
Prop. VGG + SLF-LSTM	LF	99.75%	100%	72.33%	99.00%	92.00%	89.10%
Prop. VGG + SeqL-LSTM	LF	99.75%	100%	73.17%	99.50%	92.33%	89.55%

Table 2: Protocol 2 assessment: Face recognition rank-1 for the proposed and benchmarking recognition solutions (proposed solutions and best results in bold).

Face recognition solution		Recognition Tasks					
		Neutral &emotion	Action	Pose	Illumination	Occlusion	Average
Name	Type						
PCA [40]	2D	66.00%	63.50%	16.50%	46.50%	36.00%	40.70%
LBP [42]	2D	71.00%	73.00%	21.50%	43.00%	36.50%	43.85%
HOG [41]	2D	81.50%	77.50%	21.00%	70.50%	64.00%	58.25%
VGG-Face [25]	2D	91.75%	86.00%	82.00%	90.00%	63.67%	79.65%
DLBP [43]	LF	89.50%	89.00%	72.50%	65.00%	63.33%	73.60%
MPCA [44]	LF	68.50%	68.50%	20.50%	32.00%	41.00%	42.85%
LFLBP [16]	LF	67.00%	70.50%	38.50%	46.00%	55.67%	53.75%
HOG+HDG [17]	LF	80.00%	79.00%	21.34%	67.50%	65.00%	59.20%
VGG-D ³ [18]	LF	97.25%	93.00%	86.34%	96.00%	72.33%	85.95%
VGG + Conv-LSTM [19]	LF	98.50%	99.00%	92.00%	98.00%	83.00%	91.95%
Prop. VGG + GLF-LSTM	LF	98.75%	99.50%	93.17%	98.50%	84.00%	92.80%
Prop. VGG + SLF-LSTM	LF	98.75%	99.50%	93.50%	98.50%	85.17%	93.15%
Prop. VGG + SeqL-LSTM	LF	99.25%	99.00%	94.00%	98.50%	85.17%	93.35%

Table 3: Protocol 3 assessment: Face recognition rank-1 for the proposed and benchmarking recognition solutions (proposed solutions and best results in bold).

Face recognition solution		Recognition Tasks					
		Neutral &emotion	Action	Pose	Illumination	Occlusion	Average
Name	Type						
PCA [40]	2D	53.00%	65.00%	56.66%	65.00%	56.66%	49.80%
LBP [42]	2D	48.50%	83.00%	67.66%	64.00%	67.66%	52.20%
HOG [41]	2D	51.50%	96.00%	84.66%	75.00%	84.66%	64.60%
VGG-Face [25]	2D	93.50%	97.00%	97.00%	95.00%	97.00%	92.90%
DLBP [43]	LF	56.50%	64.00%	69.66%	75.00%	69.66%	63.70%
MPCA [44]	LF	48.00%	89.00%	65.00%	63.00%	64.66%	50.30%
LFLBP [16]	LF	52.50%	96.00%	87.66%	76.00%	87.66%	65.80%
HOG+HDG [17]	LF	61.00%	93.00%	83.33%	80.00%	83.33%	67.10%
VGG-D ³ [18]	LF	94.00%	98.00%	98.00%	97.00%	98.33%	97.40%
VGG + Conv-LSTM [19]	LF	100%	100%	96.33%	100%	98.66%	98.60%
Prop. VGG + GLF-LSTM	LF	100%	100%	97.33%	100%	98.66%	98.80%
Prop. VGG + SLF-LSTM	LF	100%	100%	98.00%	100%	98.33%	98.90%
Prop. VGG + SeqL-LSTM	LF	100%	100%	98.33%	100%	98.33%	99.00%

4.6. Complexity and Compactness Analysis

This section assesses the computational complexity and memory efficiency for the proposed recognition solutions. The computational complexity is assessed by the execution times measured on a standard 64-bit Intel PC with a 3.40 GHz processor, 16 GB RAM, and a GeForce GTX 1060 graphics card, running MATLAB R2015b on Windows 10 for non-deep learning based solutions and running PyTorch with CUDA 8 toolkit on UBUNTU 16.04 for deep learning based solutions.

Error! Reference source not found. shows both i) the training times (in seconds) for the spatial description/learning, (spatio-)angular description learning, and classifier learning; and ii) the testing times (in seconds) for the spatial description, (spatio-)angular learning, and classification time, for the proposed solutions and the 10 benchmarking recognition solutions considered. Naturally, there is no angular description/learning time for non-light field based (2D) solutions. This table also summarizes the final description size in terms of the number of elements and memory size in bytes for the various solutions as this value is relevant to analyze memory efficiency. The times have been measured for each input image, either 2D or light field.

As can be observed from **Error! Reference source not found.**, the proposed recognition solutions offer the most compact representations when compared with the benchmarking solutions with best recognition accuracy, i.e., [18] and [19], thus simplifying the storage, retrieval, and transmission of the created spatio-angular descriptions. Moreover, they offer the lowest classification times during the testing phase in comparison with the benchmarking solutions. Additionally, the recognition solutions adopting the proposed LSTM cell architectures offer the fastest testing time, of less than half a second per each light field image, facilitating their operation in real-time, notably when compared with

the benchmarking solutions with best recognition accuracy. It is worthwhile to mention that the very high angular description time for [44] and [18] is the result of disparity and depth maps extraction, which are computationally very expensive.

Table 4: Average training and testing times, and description size for the proposed and benchmarking face recognition solutions (minimum values in bold).

Face recognition solution		Type	Training time(s) / image			Testing time(s) / image			Description size	
Descriptor	Classifier		Spatial description/learning	(Spatio-)angular description/learning	Classifier learning	Spatial description	(Spatio-)angular description	Classification	(number of elements)	(bytes)
PCA [40]	SVM	2D	0.149	N/A	0.025	0.149	N/A	0.018	4,095	1764
LBP [42]	SVM	2D	0.013	N/A	0.040	0.013	N/A	0.030	4,096	1801
HOG [41]	SVM	2D	0.107	N/A	0.070	0.107	N/A	0.040	8,100	60773
VGG-Face [25]	SVM	2D	0.016	N/A	0.030	0.016	N/A	0.020	4,096	15473
DLBP [43]	SVM	LF	0.026	391.061	0.492	0.026	391.061	0.271	73,728	11116
MPCA [44]	SVM	LF	0.149	0.141	0.029	0.149	0.141	0.022	4,095	1764
LFLBP [16]	SVM	LF	0.013	0.023	0.430	0.013	0.023	0.240	65,536	7581
HOG+HDG[17]	SVM	LF	0.302	0.195	0.170	0.302	0.195	0.080	16,200	122134
VGG-D ³ [18]	SVM	LF	0.048	397.473	0.150	0.048	397.473	0.100	16,384	28911
VGG + Conv-LSTM [19]	Soft max	LF	0.480	0.295	0.033	0.480	0.031	0.002	7680	29011
Prop. VGG + GLF-LSTM	Soft max	LF	0.480	0.485	0.035	0.480	0.016	0.001	3,840	14505
Prop. VGG + SLF-LSTM	Soft max	LF	0.480	0.486	0.035	0.480	0.016	0.001	3,840	14505
Prop. VGG + SeqL-LSTM	Soft max	LF	0.480	0.489	0.036	0.480	0.018	0.001	3,840	14505

4.7. Parallelization Analysis

The parallelization capabilities of modern processors and compilers can accelerate the execution time of the proposed LSTM cell architectures. The proposed LSTM cell architectures include a series of operations, described in Equations 9-22, 23-36, and 37-49, for the GLF-LSTM, SLF-LSTM and SeqL-LSTM cell architectures, respectively, with different sets of dependencies. To minimize the execution time independent operations can be run in parallel. In this context, Figure 11 shows directed acyclic graphs (DAG) for the Conv-LSTM cell architecture (Figure 11.a) as well as for the proposed GLF-LSTM (Figure 11.b), SLF-LSTM (Figure 11.c) and SeqL-LSTM (Figure 11.d) cell architectures, showing the respective operation scheduling constraints based on their dependencies. In a DAG, each node corresponds to an operation and each edge represents the dependency between two operations, where the first node's operation must be completed to feed the second node. The operations in the same level can be executed in parallel (if enough processing units are available) and the depth of the DAG can represent the number of serial phases needed to complete the whole task. Additionally, the operations highlighted by the same color have the same computational complexity as they perform the same operation, with the blue and green nodes corresponding to the most and the least complex operations, respectively.

As can be concluded from the analysis of Figure 11, although the proposed LSTM cell architectures can provide much richer descriptions, their execution times in parallel mode would only be slightly larger than the conventional LSTM cell architecture. Compared to the Conv-LSTM cell architecture, the GLF-LSTM and SLF-LSTM cell architectures have only one additional computational level, corresponding to addition operations (green nodes in Figure 11) with minimum complexity. For the SeqL-LSTM cell architecture, there are two additional computational levels with low complexity that should not add much complexity to the Conv-LSTM cell architecture. The parallelization of the proposed LSTM cell architectures can be done by: i) using 8 processing units/cores, currently available on most modern processors; and ii) preparing the code to run in parallel, respecting the scheduling constraints between the operations as presented in Figure 11.

It should also again be noted that each cell in the proposed LSTM networks accepts two view descriptions as input, one from the horizontal and another from the vertical multi-view description sequences, which is not the case for the Conv-LSTM architecture, where one LSTM cell only handles one single view description, horizontal or vertical. This

implies that the Conv-LSTM architecture requires twice the number of cells when compared to the novel LSTM cell architectures. With the assumption that Conv-LSTM cell architecture complexity is C and the number of views is N , the computational complexity of a conventional LSTM network would be $C \times N$. Considering the additional computational levels needed for the proposed LSTM cell architectures, as shown in Figure 11, and the assumption of having the same complexity for all computational levels (to analyze the worst-case complexity), the GLF-LSTM, SLF-LSTM, and SeqL-LSTM single cell architectures complexities would be $\frac{4}{3}C$, $\frac{4}{3}C$, and $\frac{5}{3}C$, respectively, since the GLF-LSTM, SLF-LSTM, and SeqL-LSTM cell architectures when compared to the Conv-LSTM have 1, 1, and 2 additional computational levels, respectively. The assumption of same complexity for all computational levels is made for simplicity; in fact, the complexity of the additional levels is considerably lower than that of the base levels. Considering that the novel cell architectures only need $\frac{N}{2}$ LSTM cells (as each simultaneously processes two views), the complexity of the proposed LSTM networks, adopting GLF-LSTM, SLF-LSTM, and SeqL-LSTM cell architectures, would be, respectively, $\frac{2}{3} \times C \times N$, $\frac{2}{3} \times C \times N$, and $\frac{2.5}{3} \times C \times N$. Hence, a parallel implementation of the proposed LSTM cell architectures should result in a lower execution time than adopting the conventional Conv-LSTM cell architecture.

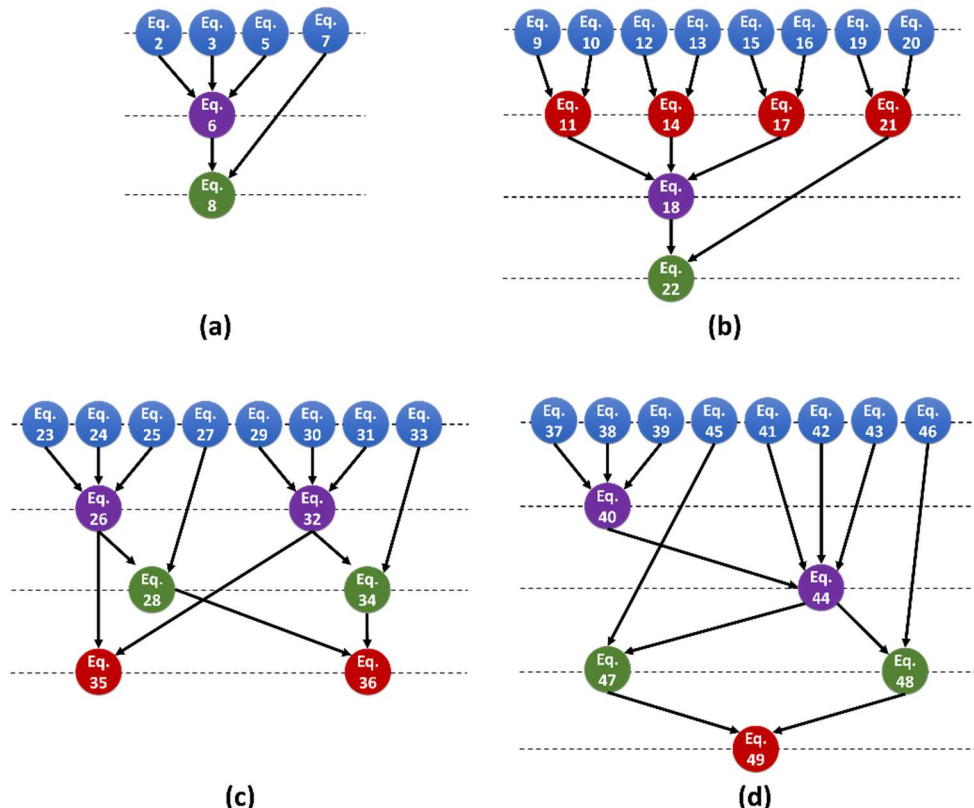


Figure 11: Directed acyclic graphs for the following LSTM cell architectures showing scheduling constraints between the operations (a) Conv-LSTM; (b) GLF-LSTM; (c) SLF-LSTM; (d) SeqL-LSTM.

5. Summary and Future Work

This paper proposes three novel LSTM cell architectures able to jointly learn a description model from the light field horizontal and vertical parallaxes. The proposed LSTM cell architectures adopt gate-level fusion, state-level fusion, and sequential learning, respectively, to provide richer angular light field descriptions to be used for several visual analysis tasks. The proposed LSTM cell architectures have been tested in the context of a spatio-angular deep learning framework for light field face recognition, with the LSTM network taking as input VGG-Face deep spatial descriptions computed for horizontal and vertical SA image sequences derived from a light field image. A comprehensive evaluation has been conducted on the IST-EURECOM LFFD using three challenging test protocols. The obtained results show the superiority of the recognition solutions based on the proposed LSTM cell architectures over 10 state-of-the-art benchmarking solutions. Additionally, the proposed solutions can offer very compact representations with rather low testing times and good parallelization ability.

The proposed LSTM cell architectures have been used for light field based face recognition in the context of this paper. As the proposed LSTM cell architectures are generic enough to address different visual recognition tasks that accept as input two related sequences, future work will consider the usage of these cell architectures for other recognition tasks.

References

- [1] J. Schmidhuber, "Deep learning in neural networks: An overview," *Neural Networks*, vol. 61, no. 1, pp. 85-117, Jan. 2015.
- [2] S. Herath, M. Harandi and F. Porikli, "Going deeper into action recognition: A survey," *Image and Vision Computing*, vol. 60, no. 1, pp. 4-21, Apr. 2017.
- [3] Z. Lipton, J. Berkowitz and C. Elkan, "A critical review of recurrent neural networks for sequence learning," arXiv:1506.00019, Oct. 2015.
- [4] S. Hochreiter and J. Schmidhuber, "Long short-term memory," *Neural Computation*, vol. 9, no. 8, pp. 1735-1780, Nov. 1997.
- [5] K. Greff, R. Srivastava, J. Koutník, B. Steunebrink and J. Schmidhuber, "LSTM: A search space odyssey," *IEEE Transactions on Neural Networks and Learning Systems*, vol. 28, no. 10, pp. 2222-2232, Oct. 2017.
- [6] S. Merity, N. Keskar and R. Socher, "Regularizing and optimizing LSTM language models," arXiv:1708.02182, Ithaca, NY, USA, Aug. 2017.
- [7] J. Donahue, L. Hendricks, M. Rohrbach, S. Venugopalan, S. Guadarrama, K. Saenko and T. Darrell, "Long-term recurrent convolutional networks for visual recognition and description," *IEEE Transactions on Pattern Analysis and Machine Intelligence*, vol. 39, no. 4, pp. 677-691, Apr. 2017.
- [8] A. Jain, K. Nandakumar and A. Ross, "50 years of biometric research: Accomplishments, challenges, and opportunities," *Pattern Recognition Letters*, vol. 79, no. 1, pp. 80-105, Aug. 2016.
- [9] M. Günther, L. El Shafey and S. Marcel, "2D face recognition: An experimental and reproducible research survey," Technical Report Idiap-RR-13, Martigny, Switzerland, Apr. 2017.
- [10] G. Hu, Y. Yang, D. Yi, J. Kittler, W. Christmas, S. Li and T. Hospedales, "When face recognition meets with deep learning: An Evaluation of convolutional neural networks for face recognition," in *IEEE International Conference on Computer Vision Workshop*, Santiago, Chile, Dec. 2015.
- [11] A. Sepas-Moghaddam, F. Pereira and P. Correia, "Face recognition: A novel multi-level taxonomy based survey," arXiv:1901.00713, Jan. 2019.
- [12] L. Best-Rowden, H. Han, C. Otto, B. Klare and A. Jain, "Unconstrained face recognition: Identifying a person of interest from a media collection," *IEEE Transactions on Information Forensics and Security*, vol. 9, no. 12, pp. 2144-2157, Dec. 2014.
- [13] R. Ng, M. Levoy, M. Bradif, G. Duval, M. Horowitz and P. Hanrahan, "Light field photography with a hand-held plenoptic camera," Tech Report CSTR 2005-02, Stanford, CA, USA, Feb. 2005.
- [14] M. Levoy and P. Hanrahan, "Light field rendering," in *23rd Annual Conference on Computer Graphics and Interactive Techniques*, New York, NY, USA, Aug. 1996.
- [15] R. Raghavendra, K. Raja and C. Busch, "Exploring the usefulness of light field cameras for biometrics: An empirical study on face and iris recognition," *IEEE Transaction on Information Forensics and Security*, vol. 11, no. 5, pp. 922-936, May 2016.
- [16] A. Sepas-Moghaddam, P. Correia and F. Pereira, "Light field local binary patterns description for face recognition," in *IEEE International Conference on Image Processing*, Beijing, China, Sep. 2017.
- [17] A. Sepas-Moghaddam, F. Pereira and P. Correia, "Ear recognition in a light field imaging framework: A new perspective," *IET Biometrics*, vol. 7, no. 3, p. 224-231, May. 2018.
- [18] A. Sepas-Moghaddam, P. Correia, K. Nasrollahi, T. Moeslund and F. Pereira, "Light field based face recognition via a fused deep representation," in *IEEE International Workshop on Machine Learning for Signal Processing*, Aalborg, Denmark, Sep. 2018.
- [19] A. Sepas-Moghaddam, M. Haque, P. Correia, K. Nasrollahi, T. Moeslund and F. Pereira, "A double-deep spatio-angular learning framework for light field based face recognition," arXiv:1805.10078, Dec. 2018.
- [20] R. Raghavendra, K. Raja and C. Busch, "Presentation attack detection for face recognition using light field camera," *IEEE Transactions on Image Processing*, vol. 24, no. 3, pp. 1060-1075, Mar. 2015.
- [21] A. Sepas-Moghaddam, L. Malhadas, P. Correia and F. Pereira, "Face spoofing detection using a light field imaging framework," *IET Biometrics*, vol. 7, no. 1, pp. 39-48, Jan. 2018.

- [22] A. Sepas-Moghaddam, F. Pereira and P. Correia, "Light field based face presentation attack detection: Reviewing, benchmarking and one step further," *IEEE Transactions on Information Forensics and Security*, vol. 13, no. 7, pp. 1696-1709, Jul. 2018.
- [23] A. Sepas-Moghaddam, F. Pereira and P. Correia, "Ear presentation attack detection: Benchmarking study with first lenslet light field database," in *European Signal Processing Conference*, Rome, Italy, Sep. 2018.
- [24] V. Chiesa and J. Dugelay, "Advanced face presentation attack detection on light field database," in *International Conference of the Biometrics Special Interest Group*, Darmstadt, Germany, Sep. 2018.
- [25] O. Parkhi, A. Vedaldi and A. Zisserman, "Deep face recognition," in *British Machine Vision Conference*, Swansea, UK, Sep. 2015.
- [26] A. Sepas-Moghaddam, V. Chiesa, P. Correia, F. Pereira and J. Dugelay, "The IST-EURECOM light field face database," in *International Workshop on Biometrics and Forensics*, Coventry, UK, Apr. 2017.
- [27] E. Adelson and J. Bergen, "The plenoptic function and the elements of early vision," in *Computation Models of Visual Processing*, Cambridge, MA, USA, MIT Press, 1991, pp. 3-20.
- [28] M. Levoy and P. Hanrahan, "Light field rendering," in *23rd Annual Conference on Computer Graphics and Interactive Techniques*, New York, NY, USA, Aug. 1996.
- [29] S. Gortler, R. Grzeszczuk, R. Szeliski and M. Cohen, "The lumigraph," in *Annual Conference on Computer Graphics and Interactive Techniques*, New Orleans, LA, USA, Aug. 1996.
- [30] D. Dansereau, "Plenoptic signal processing for robust vision in field robotics," PhD Thesis in Mechatronic Engineering, Queensland University of Technology, Queensland, Australia, Jan. 2014.
- [31] B. Wilburn, "High performance imaging using arrays of inexpensive cameras," PhD Thesis in Department of Electrical Engineering, Stanford University, Stanford, CA, USA, Dec. 2004.
- [32] ISO/IEC JTC 1/SC 29/WG 1, "JPEG pleno call for proposals on light field coding," ISO/IEC, Geneva, Switzerland, Jan. 2017.
- [33] R. Ng, M. Levoy, M. Bradif, G. Duval, M. Horowitz and P. Hanrahan, "Light field photography with a hand-held plenoptic camera," Tech Report CSTR 2005-02, 2005.
- [34] F. Pereira and E. Silva, "Efficient plenoptic imaging representation: Why do we need it?," in *IEEE International Conference on Multimedia and Expo*, Seattle, WA, USA, Jul. 2016.
- [35] P. Werbos, "Backpropagation through time: What it does and how to do it," *Proceedings of the IEEE*, vol. 78, no. 10, pp. 1550-1560, Oct. 1990.
- [36] S. Hochreiter, "The vanishing gradient problem during learning recurrent neural nets and problem solutions," *International Journal of Uncertainty, Fuzziness and Knowledge-Based Systems*, vol. 6, no. 2, pp. 107-116, Apr. 1998.
- [37] K. Simonyan and A. Zisserman, "Very deep convolutional networks for large-scale image recognition," arXiv preprint arXiv:1409.1556, Ithaca, NY, USA, Apr. 2015.
- [38] D. Dansereau, "Light Field Toolbox V. 0.4," [Online]. Available: <http://www.mathworks.com/matlabcentral/fileexchange/49683-light-field-toolbox-v0-4>. [Accessed Oct. 2018].
- [39] "Lytro website," Lytro Inc, [Online]. Available: <https://www.lytro.com>. [Accessed Oct. 2018].
- [40] M. Turk and A. Pentland, "Eigenfaces for recognition," *Journal of Cognitive Neuroscience*, vol. 3, no. 1, pp. 71-86, Jan. 1991.
- [41] O. Déniz, G. Bueno, J. Salido and F. De la Torre, "Face recognition using histograms of oriented gradients," *Pattern Recognition Letters*, vol. 32, no. 12, pp. 1598-1603, Sep. 2011.
- [42] G. Zhao, T. Ahonen, J. Matas and M. Pietikainen, "Rotation-invariant image and video description with local binary pattern features," *IEEE Transactions on Image Processing*, vol. 21, no. 4, pp. 1465-1467, Apr. 2012.
- [43] A. Aissaoui, J. Martinet and C. Djeraba, "DLBP: A novel descriptor for depth image based face recognition," in *IEEE International Conference on Image Processing*, Paris, France, Oct. 2014.
- [44] H. Lu, K. Plataniotis and A. Venetsanopoulos, "MPCA: Multilinear principal component analysis of tensor objects," *IEEE Transactions on Neural Networks*, vol. 19, no. 1, pp. 18-39, Jan. 2008.
- [45] S. Marto, N. Monteiro, J. Barreto and J. Gaspar, "Structure from plenoptic imaging," in *IEEE International Conference on Development and Learning and on Epigenetic Robotics*, Lisbon, Portugal, Sep. 2017.
- [46] N. Monteiro, S. Marto, J. Barreto and J. Gaspar, "Depth range accuracy for plenoptic cameras," *Computer Vision and Image Understanding*, vol. 168, no. 1, pp. 104-117, Mar. 2018.
- [47] H. Jeon, J. Park, G. Choe and G. Park, "Accurate depth map estimation from a lenslet light field camera," in *IEEE International Conference on Computer Vision and Pattern Recognition*, Boston, MA, USA, Jun. 2015.